

Article

Study of the Radiation Damage Kinetics in NbTiVZr High-Entropy Alloys Irradiated by Heavy Ions

Kayrat K. Kadyrzhanov ¹, Artem L. Kozlovskiy ^{1,2,*}, Dmitriy I. Shlimas ^{1,3}, Daryn B. Borgekov ^{1,3}, Sholpan G. Giniyatova ¹, Vladimir V. Uglov ⁴ and Maxim V. Zdorovets ^{1,3,5}

¹ Engineering Profile Laboratory, L.N. Gumilyov Eurasian National University, Satpayev St., Astana 010008, Kazakhstan

² Department of General Physics, Satbayev University, Almaty 050032, Kazakhstan

³ Laboratory of Solid State Physics, The Institute of Nuclear Physics, Almaty 050032, Kazakhstan

⁴ Department of Solid State Physics, Belarusian State University, 220050 Minsk, Belarus

⁵ Department of Intelligent Information Technologies, Ural Federal University, Yekaterinburg 620075, Russia

* Correspondence: kozlovskiy.a@inp.kz; Tel./Fax: +77-024-4133-68

Abstract: The purpose of this paper was to study the kinetics of accumulation of radiation damage in the near-surface layer of a high-entropy NbTiVZr alloy upon irradiation with heavy Kr¹⁵⁺ ions and fluences of 10¹⁰–10¹⁵ ion/cm². According to the data of X-ray diffraction analysis, it was found that irradiation with heavy ions lead to structural changes associated with the accumulation of deformation distortions and stresses. In this case, the nature of deformation distortions was associated with tensile distortions of the crystal lattice and swelling of the near-surface layer. An analysis of the strength properties of the irradiated samples showed that the accumulation of deformation distortions in the near-surface layer lead to a decrease in the resistance to cracking and destruction of the near-surface layer. In this case, the main changes occurred at fluences above 10¹³ ion/cm², which are characterized by an excess of the threshold for overlapping defective regions that appear along the trajectory of incident ions. Tribological tests showed that an increase in defective inclusions in the structure of the near-surface layer lead to an increase in friction and a decrease in crack resistance.



Citation: Kadyrzhanov, K.K.; Kozlovskiy, A.L.; Shlimas, D.I.; Borgekov, D.B.; Giniyatova, S.G.; Uglov, V.V.; Zdorovets, M.V. Study of the Radiation Damage Kinetics in NbTiVZr High-Entropy Alloys Irradiated by Heavy Ions. *Metals* **2023**, *13*, 727. <https://doi.org/10.3390/met13040727>

Academic Editor: Duc Nguyen-Manh

Received: 14 March 2023

Revised: 3 April 2023

Accepted: 5 April 2023

Published: 7 April 2023



Copyright: © 2023 by the authors. Licensee MDPI, Basel, Switzerland. This article is an open access article distributed under the terms and conditions of the Creative Commons Attribution (CC BY) license (<https://creativecommons.org/licenses/by/4.0/>).

1. Introduction

In the last decade, much attention was paid to the development of advanced structural materials for the construction and further operation of new generation nuclear reactors, including fast neutron reactors and high-temperature reactors [1–3]. Interest in new types of reactor plants is primarily due to the need to remove a number of restrictions that are typical for light water reactors of generations II and III. The limitations primarily stem from the inability to develop closed fuel cycle reactors, which are instrumental in reducing the production of long-lasting nuclear waste by increasing the degree of nuclear fuel burn up [4,5]. Additionally, innovative nuclear facilities suggest using helium or sodium as coolants to elevate the core temperature, thereby improving reactor efficiency [6,7].

As a rule, the operation of structural materials for new types of nuclear reactors implies exposure to high temperatures, mechanical stresses and loads, as well as thermal effects. At the same time, the most critical condition for the use of new types of structural materials is their high stability of properties that can withstand extreme impacts, including high-dose irradiation not only with neutron fluxes, but also with fission products of nuclear fuel [8–10]. At the same time, these requirements apply both to materials that are planned to be used in the core and outside it [11–13]. In turn, new types of structural materials used in the core must simultaneously withstand large thermal loads (500–700 °C), dose loads from neutrons and fission fragments, and also be resistant to the coolant (sodium or helium). For structural

materials of the inactive zone, the main operating conditions are associated with long-term thermal exposure (up to 600 °C), a long service life (up to 40–50 years), as well as exposure to a coolant that can lead to destruction of the near-surface layer [14–17]. To solve these problems, a number of materials were recently proposed, including austenitic stainless steels, ceramics, and high-entropy alloys, which are able to meet all the requirements for structural materials of new generation reactors (Generation IV) [18–21]. Additionally, one of the promising and frequently used materials as structural materials is silicon carbide, which, due to its physicochemical and strength properties, as well as high radiation resistance at high temperature irradiation, is considered as a candidate material for the core [22].

In turn, the interest in high-entropy alloys is due to a wide variety of various practical applications associated with the high resistance of alloys to external influences [23,24]. At the same time, great attention is paid to the use of high-entropy alloys for operation at an increased radiation background, including the effect of heavy ions, neutrons, and high temperatures. At the same time, the choice of the concept of using metals with a high melting point, such as tungsten, tantalum, molybdenum, titanium, niobium, zirconium, and vanadium, allows solving a number of issues in the field of operation of structural materials under extreme conditions [25–27].

Based on the foregoing, the main goal of this study is to establish the relationship between the accumulation of radiation damage caused by irradiation with heavy ions and structural and strength changes in the near-surface damaged layer, the change of which can lead to negative consequences during operation. High-entropy NbTiVZr, which has increased strength and resistance to mechanical stress, was chosen as the object of research, which makes it one of the candidate structural materials for the core of nuclear reactors, as well as fuel cell materials. The choice of the type of heavy Kr¹⁵⁺ ions with an energy of 147 MeV and radiation fluences of 10^{10} – 10^{15} ion/cm² is due to the possibility of simulation of radiation damage comparable to the impact of fission fragments of nuclear fuel in the core of a nuclear reactor. Additionally, considering the maximum penetration depth of ions in the material and the particle flow, it is possible to simulate the effect of neutron exposure at a given depth of the damaged layer.

2. Experimental Method

The high-entropy NbTiVZr alloy with an equiatomic composition and a density close to 6.5 g/cm³ was chosen as the object of study. The choice of this alloy was due to its high strength characteristics, as well as good ductility and resistance to temperature effects.

The samples were obtained from chemically pure elements Nb, Ti, V, and Zr (chemical purity 99.9%) using the arc melting method in a copper furnace. The vacuum in the furnace was at least 5×10^{-5} mbar. To achieve a homogeneous distribution of elements in the alloy, the samples were subjected to melting at least 5 times. According to X-ray diffraction data, the resulting NbTiVZr alloy was characterized by a body-centered cubic lattice with a high structural ordering degree. Samples for further testing to determine the effect of radiation damage to the near-surface layer on the change in strength properties were plates that were 10 × 10 mm in size and 100 μm thick with a polished surface. Figure 1 shows the appearance of the samples used for irradiation after polishing. Morphological features were analyzed using scanning electron and atomic force microscopy. To carry out these studies, a Hitachi TM 3030 scanning electron microscope (Hitachi, Tokyo, Japan) and an AIST-NT atomic force microscope (AIST-NT, Inc., Phoenix, AZ, USA) were used. As can be seen from the presented data, the surface roughness of the samples after polishing was no more than 20–30 nm.

Irradiation of samples of high-entropy alloys in order to establish resistance to radiation damage caused by heavy ions was carried out at the DC-60 heavy ion accelerator (Astana, Kazakhstan). Kr¹⁵⁺ ions with an energy of 147 MeV were chosen as heavy ions, the irradiation fluence was from 10^{10} to 10^{15} ion/cm², and the ion flux density was no more than 10^9 ion/cm²·s. The choice of irradiation conditions, as well as the type of heavy ions, was due to the possibility of modeling radiation damage in high-entropy alloys,

comparable to damage caused by fission fragments of nuclear fuel in the core [28,29]. The range of irradiation fluences were chosen in order to assess the kinetics of accumulation of radiation damage, including the formation of single radiation defects before the formation of overlap regions and the initialization of softening processes in the damaged layer.

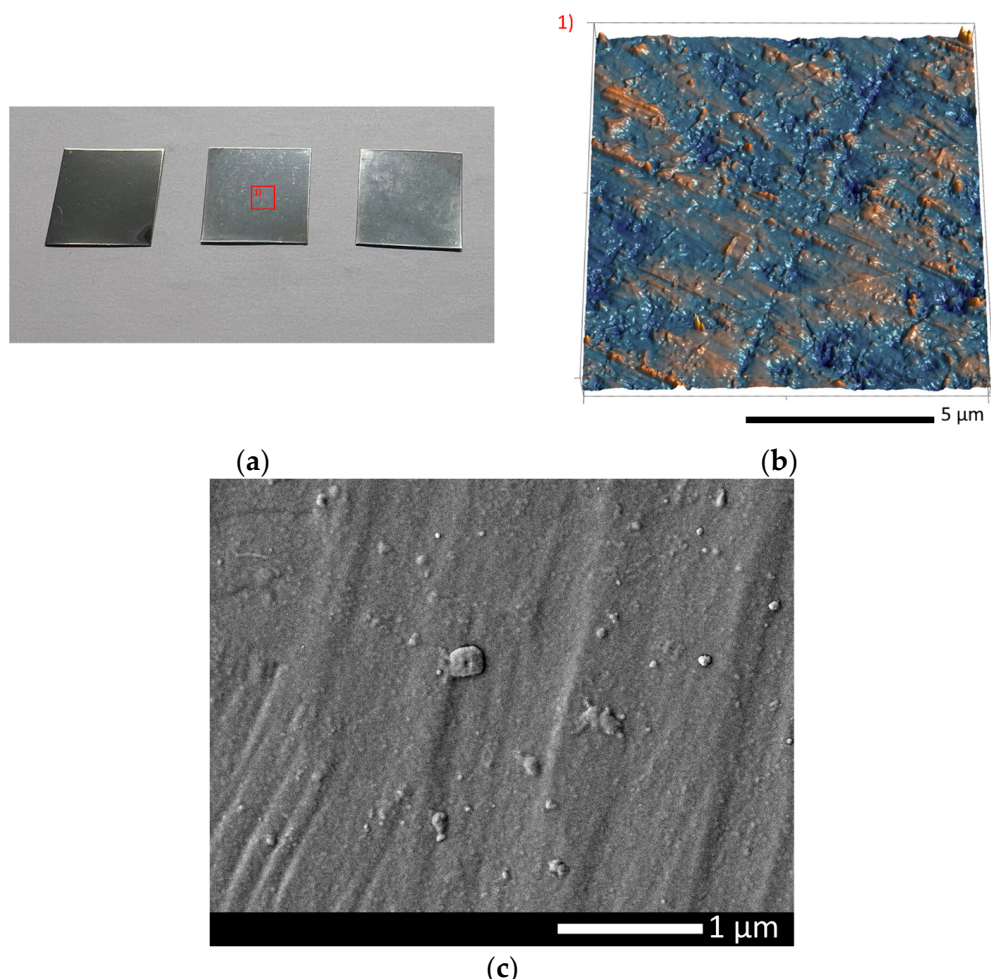


Figure 1. Data on the morphological features of the obtained samples of NbTiVZr alloys: (a) general view of the obtained samples; (b) 3D reconstruction of the sample surface after polishing; (c) SEM image of the sample surface.

Figure 2 shows the results of modeling the ionization losses of incident Kr^{15+} ions with an energy of 147 MeV in the NbTiVZr target, as well as data on the distribution of atomic displacements along the ion trajectory in the material, performed using the SRIM Pro 2013 program code. For simulation, the Kinchin–Pease model was used, taking into account the formation of cascade collisions during the interaction of incident ions with the nuclear and electronic subsystems of the target.

As can be seen from the presented calculation data, the maximum path length of Kr^{15+} ions with an energy of 147 MeV in the NbTiVZr target was approximately 12 μm . In turn, an analysis of the weight contributions of the ionization losses of incident ions during interaction with the electronic and nuclear subsystem of the alloy showed that over most of the trajectory of ion motion in the material, the main contribution to structural changes was made by the electronic ionization losses of ions, whose value was 16–17 keV/nm. It should also be noted that, in contrast to ceramics [30,31], the ionization losses for high-entropy alloys under irradiation with heavy ions were 1.5–2 times lower, which was due to the higher density of the alloys, as well as higher radiation resistance. The values of ionization losses of ions during interaction with the nuclear subsystem were approximately 0.27–0.55 keV/nm, which was two orders of magnitude less than the similar value of

ionization losses during interaction with the electronic subsystem. At the same time, these ionization losses made the main contribution to structural changes in the form of atomic displacements at a depth of 10–12 μm . Figure 1b shows the results of estimating the magnitude of atomic displacements along the ion trajectory in the target material, calculated on the basis of ionization loss data. These values of atomic displacements are presented depending on the irradiation fluence. According to the presented simulation results, it can be seen that the main changes in the structure were observed only when the maximum range of ions was reached, which was characterized by the dominance of ionization losses associated with the interaction of ions with the nuclear subsystem. At the same time, these shifts were most pronounced only in the case of reaching the maximum irradiation fluences of 10^{14} – 10^{15} ion/ cm^2 , which, according to a number of literature data, were characteristic of the effect of deep overlapping of defective regions formed during irradiation [32,33]. The results of the dependence of the irradiation fluence and the accumulated atomic displacements obtained from the calculated data of ionization losses are presented in Figure 3. Subsequently, to conduct a comparative analysis of structural and strength changes, the values of atomic displacements were used, which reflect the effect of accumulation of structural changes. As can be seen from the data presented in Figure 3, the largest achievable value of atomic displacements at a fluence of 10^{15} ion/ cm^2 was at least 0.04 dpa. The kinetics of radiation damage caused by irradiation with heavy ions was considered in the generally accepted theory of “thermal spike”, according to which, as a result of the interaction of incident ions with the target structure, a metastable local region (on the order of several nanometers in size) with a changed electron density was formed along the ion trajectory. During the formation of such a region in the structure of the material and its subsequent transformation that occurred due to the transfer of energy as a result of the electron–phonon interaction, local heating of the material occurred, leading to structural changes, including the formation of defects and deformation distortions. The consequences of the formation of such local areas, and in the case of high-dose irradiation (at fluences above 10^{12} ion/ cm^2), their overlaps are expressed in the form of structural distortions that affect the change in strength properties, as well as the resistance of materials to radiation degradation.

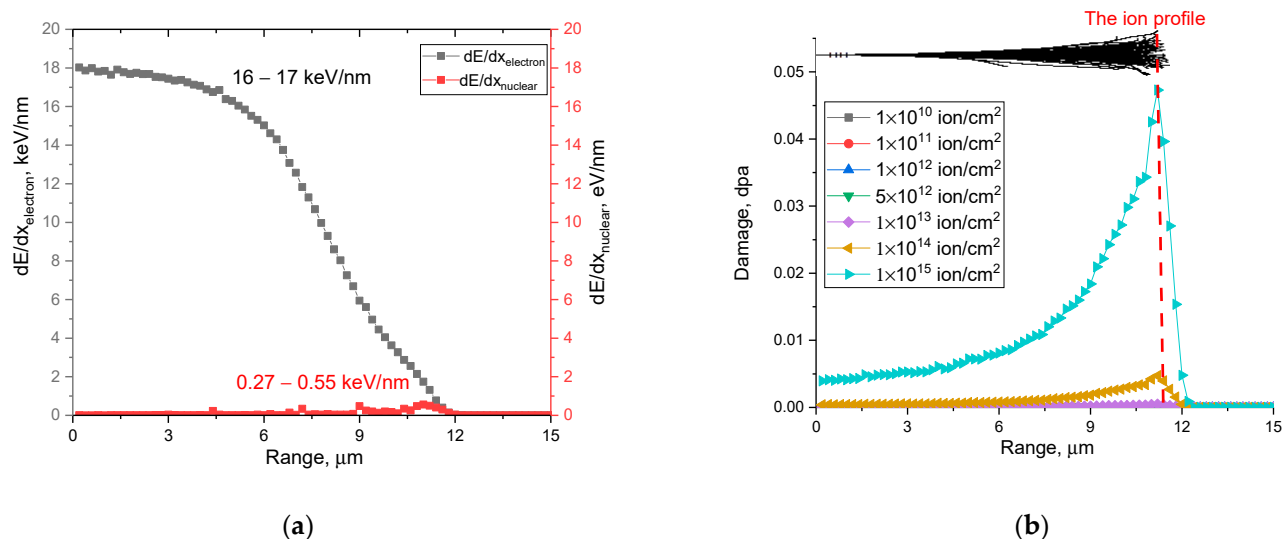


Figure 2. (a) Results of simulation of ionization losses of incident Kr^{15+} ions with an energy of 147 MeV in a NbTiVZr alloy target with a density of $6.5 \text{ g}/\text{cm}^3$. (b) Simulation results of the distribution of atomic displacements along the ion trajectory in the target material.

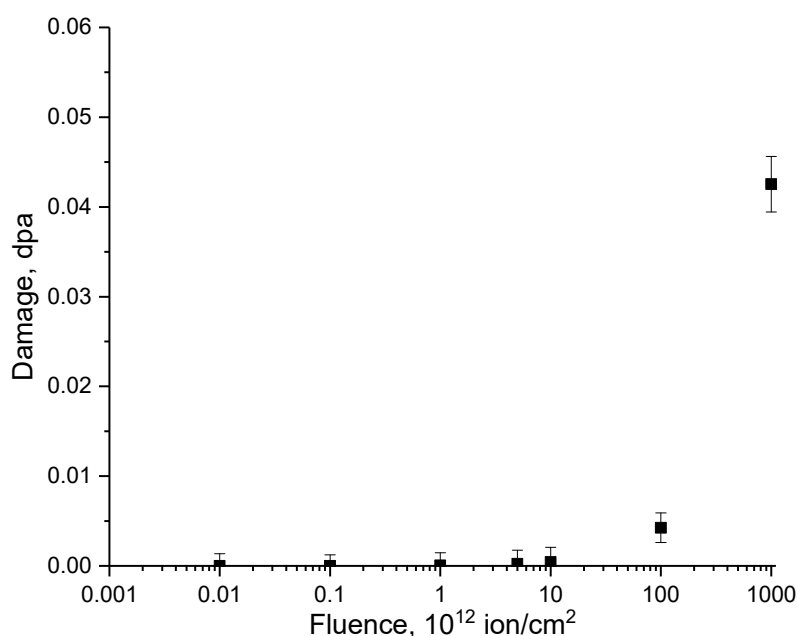


Figure 3. Dependence of the change in the value of atomic displacements depending on the irradiation fluence.

An assessment of the change in structural parameters depending on the irradiation fluence, and as a consequence of the accumulated concentration of radiation damage in the damaged layer of high-entropy NbTiVZr alloys, was carried out using the method of X-ray diffraction analysis. X-ray diffraction patterns were taken in the Bragg–Brentano geometry in the angular range of $2\theta = 30\text{--}100^\circ$, with a step of 0.03° . Determination of structural changes and distortions was evaluated by analyzing the displacement of diffraction reflections, Williamson–Hall plots were used to determine stresses, and to determine the shape of diffraction reflections. X-ray diffraction patterns were obtained using a D8 Advance ECO X-ray diffractometer (Bruker, Berlin, Germany).

The measurement of strength characteristics as a result of irradiation was studied using the indentation method to determine the hardness of the surface layer and its softening with the accumulation of radiation damage. The hardness measurement was carried out using a LECO LM700 microhardness tester (LECO, Tokyo, Japan). A Vickers diamond pyramid was used as an indenter, the pressure on the indenter was 500 N. Visual images of the surface after indentation were obtained to determine the indent geometry. Hardness tests were carried out by 25–30 successive indentations in different parts of the irradiated surface to determine the average value of the hardness index and standard deviation.

Tribological tests were carried out using the method of determining the coefficient of dry friction when rolling a ceramic ball on the surface of the sample under a load of 100 N. The number of cycles was 10,000. Wear-resistance tests were carried out by five successive measurements of the hardness index from different areas. The size of the trajectory of movement of the ceramic ball over the surface was 7 mm. The change in friction coefficient was performed after wear tests; however, in the case of irradiated specimens, the friction coefficient was evaluated in two steps. The first stage consisted in comparing the change in the value of the friction coefficient of the irradiated samples after 50–100 first test cycles, which made it possible to determine the dynamics of the change in this value of the friction coefficient depending on the accumulated radiation damage to the surface of the samples associated with a decrease in hardness and resistance to softening. The second stage of the measurements consisted in determining the value of the friction coefficient for the samples after cyclic tests.

3. Results and Discussion

Figure 4 shows the results of changes in the X-ray diffraction patterns of the studied NbTiVZr alloys depending on the fluence of irradiation with heavy Kr¹⁵⁺ ions in comparison with the X-ray diffraction pattern of the original alloy sample. According to the data of X-ray phase analysis, the resulting alloy in the initial state was characterized by a body-centered cubic lattice with a parameter $a = 3.2868 \text{ \AA}$ and a crystal lattice volume of 35.51 \AA^3 , spatial system Im-3m (229). The deformation factor of distortion of the crystal lattice of the sample in the initial state, when compared with the reference values of the parameter, was 0.023%, and the nature of the distortion was characteristic of the presence of tensile stresses in the structure of the crystal lattice, the presence of which is associated with the processes of obtaining the NbTiVZr alloy.

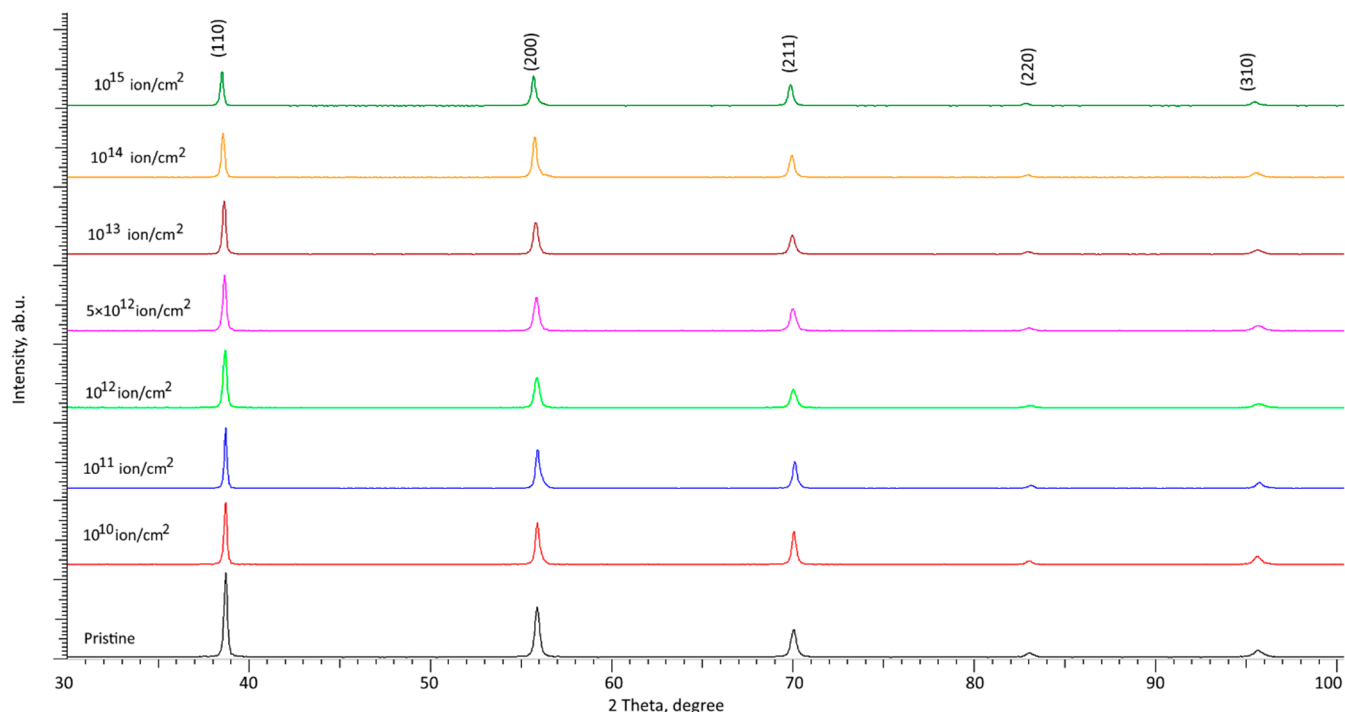


Figure 4. X-ray diffraction patterns of NbTiVZr alloys plotted against fluence of irradiation with heavy Kr¹⁵⁺ ions.

An analysis of the obtained X-ray diffraction patterns of samples of NbTiVZr alloys depending on the irradiation fluence showed the absence of any changes in diffraction reflections associated with the separation of the main peaks associated with thermal effects in the alloys during their heating, as well as the separation of solid solution phases as a result of deformation processes that were observed in [26,34]. According to the established data, the shift of diffraction reflections to the region of small angles indicates the tensile nature of the deformation of the crystal lattice [35]. This nature of the structure change as a result of irradiation was due to the effects of radiation-induced damage accumulation in the near-surface layer, as well as the possible penetration of incident ions into interstices, thereby leading to the appearance of the effect of gas-filled bubbles. Structural distortions were also due to the effects associated with atomic displacements, leading to the formation of vacancy defects, as well as the possibility of the formation of cascade collisions in the case of a large amount of energy transferred by the incident ions to the knocked out atom.

The main changes caused by irradiation were associated with a shift of diffraction reflections to the region of small angles associated with the accumulation of deformation distortions, as well as a decrease in the intensity of reflections, indicating structural disorder. At the same time, the change in the intensities of diffraction reflections was most pronounced for irradiation fluences of 10^{14} – $10^{15} \text{ ion}/\text{cm}^2$, which indicates that, at these

fluences, the formation of disordered regions was most likely, which can have a negative impact on the change in the structural and strength properties of alloys.

The results of evaluating the deformation factor, which reflects distortion of the crystal lattice of the alloys under study, depending on the amount of accumulated radiation damage, are shown in Figure 5a. The general form of the presented dependence indicates the cumulative effect of deformations of the crystal lattice, and also that the type of deformation is characteristic of tensile stresses arising during irradiation. At the same time, at low irradiation fluences (10^{10} – 5×10^{12} ion/cm²), small changes in the deformation factor indicate a high resistance of the crystal structure to deformation.

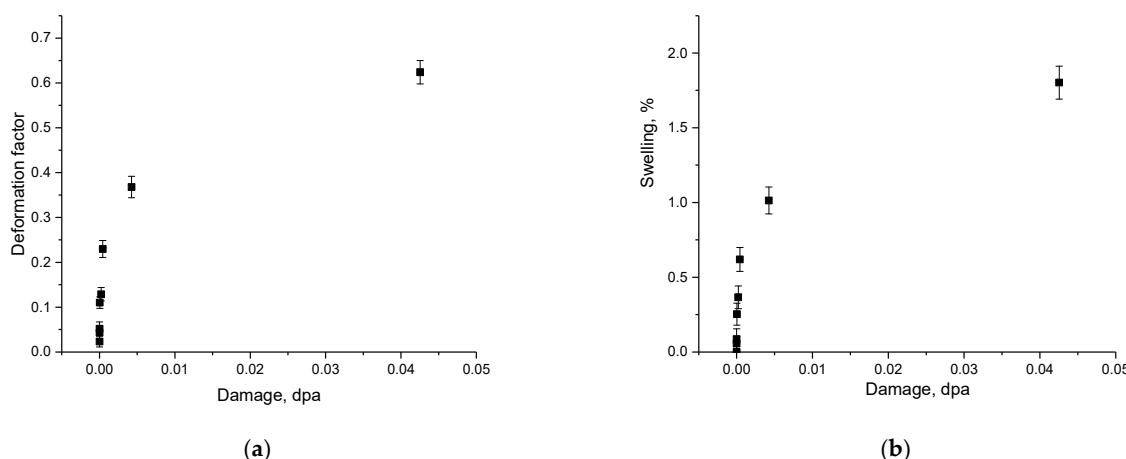


Figure 5. (a) Results of the change in the crystal lattice deformation factor depending on the value of atomic displacements; (b) results of the change in the value of the crystal lattice volume swelling on the value of atomic displacements.

Figure 5b shows the data on the change in the value of the volume swelling of the crystal lattice depending on the value of atomic displacements, calculated on the basis of the data on ionization losses with increasing irradiation fluence. The swelling was calculated on the basis of changes in the volume of the crystal lattice during the accumulation of radiation damage. The general view of the trend in the change in the magnitude of swelling of the crystal lattice on the magnitude of atomic displacements can be characterized by two stages, characterized by different swelling rates. The first stage of the change in the swelling value was typical for small changes in the displacement value (less than 0.001 dpa), and the swelling value was less than 0.5%. At the same time, an increase in the irradiation fluence above 10^{13} ion/cm² lead to a sharp increase in the swelling value above 1.0%, which indicates that the deformation distortions of the crystal lattice that occurred during the interaction of incident ions with the crystal structure exhibited an accumulation effect at high fluences. This effect, with an increase in fluence, and as a consequence of a change in the magnitude of atomic displacements, lead to an almost twofold increase in the magnitude of swelling, which is expressed in a change in the trend in Figure 5b. Additionally, swelling processes can be caused by the effect of accumulation of structural disorder in the near-surface layer, leading to partial amorphization of the crystal structure. At the same time, the nature of the change in deformation distortions and crystal lattice swelling trend indicates that the deformation distortions initiated by irradiation have a tensile character.

When estimating the areas of diffraction reflections using expression (1) [36], the amorphization (f_A) of the damaged layer structure was estimated as a result of the radiation damage accumulation. This method for evaluating amorphous inclusions in the composition of irradiated samples was based on determining the weight contribution of disordered regions in the structure of the damaged layer, the formation of which is associated with an increase in the contribution from background radiation or a change in the intensity of diffraction reflections, as well as a change in the FWHM value. Deformation distortions

were estimated from the change in the position of diffraction peaks, the change in the position of which indicates the formation of distorting factors in the structure caused by deformation of the crystal lattice, an increase or decrease in its volume. At the same time, the estimation of the shift of diffraction maxima makes it possible to estimate the nature of deformation distortions associated with the occurrence of tensile or compressive stresses in the structure of the damaged layer.

$$f_A = 1 - \frac{\sum_{i=1}^n \frac{A_i^{irrad}}{A_i^{unirrad}}}{n}, \quad (1)$$

where $A_i^{unirrad}$ and A_i^{irrad} are the contributions of diffraction reflections before and after irradiation, n is the number of diffraction reflections.

The results of changes in the content of amorphous inclusions depending on the irradiation fluence and the value of atomic displacements are shown in Figure 6a. The general view of the presented data on changes in the concentration of amorphous inclusions, as well as deformation distortions, testifies to the cumulative effect, which was most pronounced at high irradiation fluences.

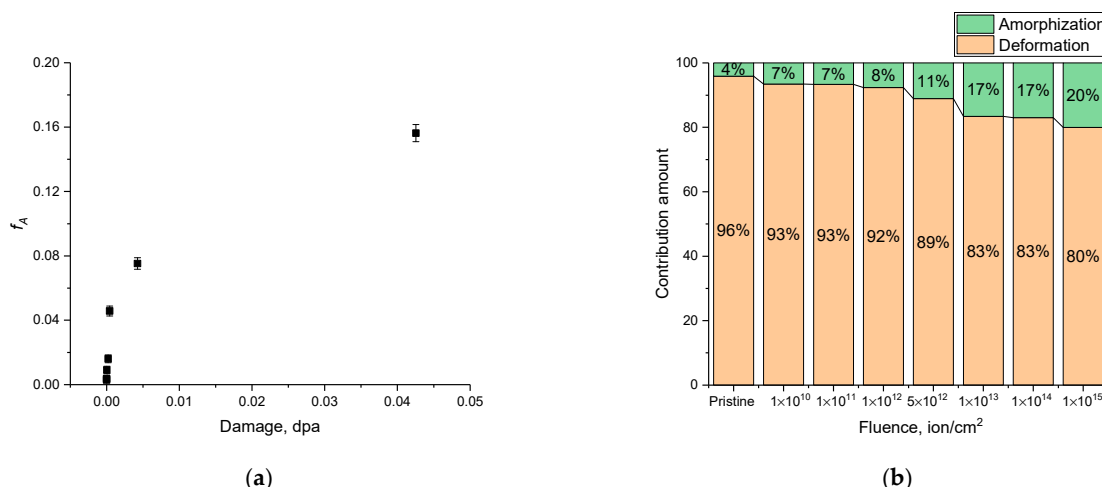


Figure 6. (a) Data on changes in the concentration of amorphous inclusions in the damaged layer of the alloy; (b) results of evaluation of the contributions of deformation distortions and amorphous inclusions in the damaged layer depending on the irradiation fluence.

The assessment of the contributions of deformation distortions and amorphous inclusions to structural changes in the near-surface damaged layer is presented in the diagram in Figure 6b.

As can be seen from the data presented, in the case of the initial samples, there was a small concentration of areas of disorder, the presence of which was due to the processes of obtaining the alloy during melting and its subsequent formation. At the same time, the deformation distortions of the crystal lattice and changes in its volume play a dominant role in structural changes. In the case of irradiated samples, the dominance of deformation distortions in structural changes was observed at low fluences, for which small changes in the contribution of amorphous inclusions or disordered regions were associated with a cumulative effect. At irradiation fluences above 5×10^{12} ion/cm², an increase in the contribution of amorphous inclusions was observed, which began to play a very significant role in the degradation of the near-surface damaged layer and its disordering, which can lead to softening and degradation of strength properties.

The evaluation of the strength properties was carried out by determining the changes in the hardness of the surface of the alloys during indentation. Figure 6 shows images of indenter prints when measuring the microhardness of the surface of the NbTiVZr alloy depending on the irradiation fluence. As can be seen from the presented data of the indenter

prints (See Figure 7), the pyramidal shape of the print was preserved for all irradiated samples, which indicates an isotropic distribution of the compression load. At the same time, in the case of high irradiation fluences (above 10^{12} ion/cm 2), wavy inclusions were clearly visible near the edges of the imprints, the area of which grew with increasing fluence. The formation of such inclusions indicates softening of the surface layer due to accumulated structural distortions and deformation inclusions, leading to cracking and a decrease in the strength characteristics of the irradiated alloys.

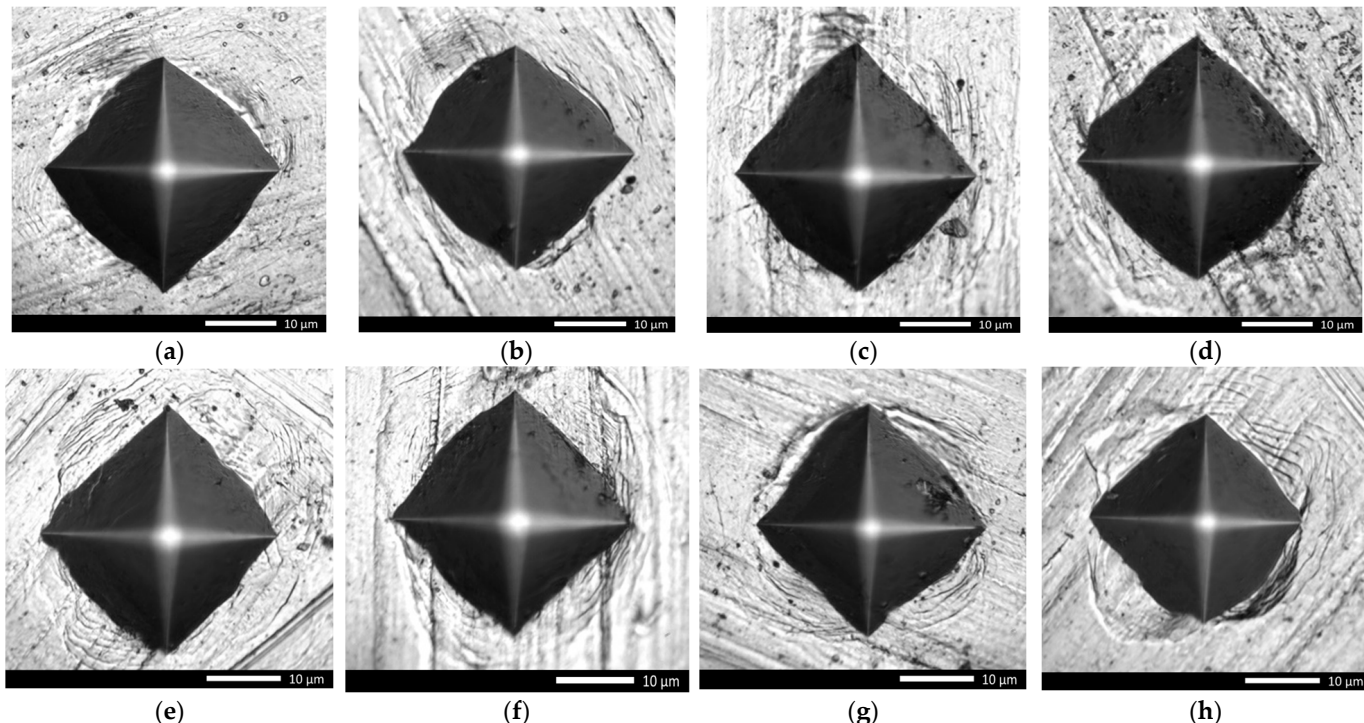


Figure 7. Image of indenter prints in NbTiVZr high-entropy alloy, made using a microhardness tester depending on the irradiation fluence: (a) initial sample; (b) 10^{10} ion/cm 2 ; (c) 10^{11} ion/cm 2 ; (d) 10^{12} ion/cm 2 ; (e) 5×10^{12} ion/cm 2 ; (f) 10^{13} ion/cm 2 ; (g) 10^{14} ion/cm 2 ; (h) 10^{15} ion/cm 2 .

Figure 8 shows the results of changes in the hardness of the near-surface layer depending on the magnitude of atomic displacements during irradiation with heavy Kr $^{15+}$ ions. The results of the obtained values reflect changes in the strength properties during the radiation damage accumulation, as well as the associated softening during deformation. As can be seen from the data presented, the most pronounced changes in the hardness value were observed when the atomic displacements exceeded 0.0001 dpa, which are typical for fluences of 10^{14} – 10^{15} ion/cm 2 . The presence of the effect of small changes at atomic displacements less than 0.0001 dpa was due to the possibility of a slight increase in the dislocation density, which prevents softening and the formation of microcracks and cleavages under external influences, thereby leading to the strengthening of the near-surface damaged layer [37].

Figure 9 presents the results of a comparative analysis of changes in the values of the near-surface layer softening and its amorphization during the accumulation of radiation damage and atomic displacements in the case of irradiation with heavy Kr $^{15+}$ ions. The softening of the near-surface layer was estimated from the change in the surface hardness of the alloy of the irradiated samples in comparison with the initial value. The amorphization degree is presented as a percentage calculated on the basis of Equation (1).

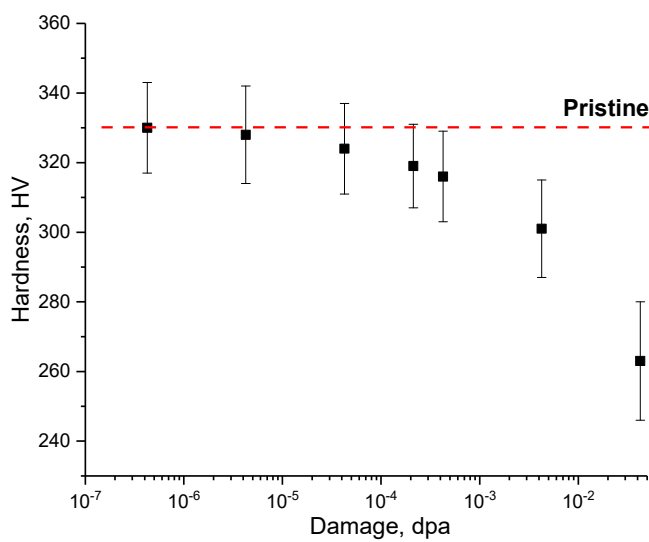


Figure 8. Results of changes in hardness depending on the value of atomic displacements upon irradiation with heavy Kr¹⁵⁺ ions (data are presented on a logarithmic scale).

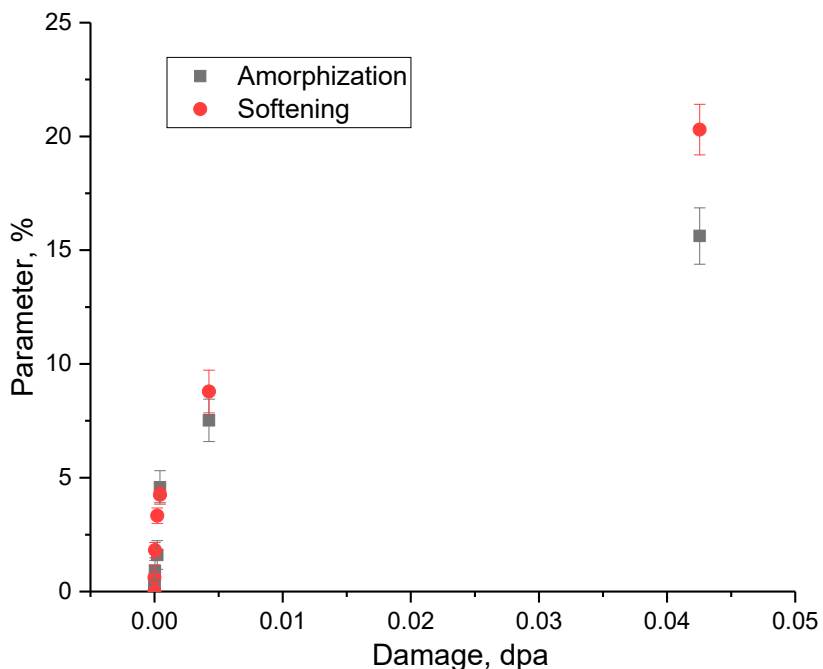


Figure 9. Correlation between changes in amorphization and softening of the damaged layer on the magnitude of atomic displacements upon irradiation with heavy Kr¹⁵⁺ ions.

According to the data obtained, a correlation was observed between the change in the strength properties of the near-surface damaged layer and the change in the amount of amorphization, which increased with the accumulation of radiation damage and their subsequent evolution. In this case, the greatest changes in the strength properties were observed for an irradiation fluence of 10^{15} ion/cm², which is characteristic of the effects of deep overlapping of defective regions that arise along the ion motion trajectory in materials [38]. The established relationship between changes in strength characteristics and accumulated amorphous inclusions indicated that the formation of highly disordered amorphous regions in the surface layer had the greatest effect on softening, the presence of which can lead to partial embrittlement and cracking.

Figure 10 demonstrates the results of tribological tests of the studied samples of high-entropy alloys subjected to irradiation with different fluences. Figure 9b also shows the

results of the evaluation of the profile after rolling, which reflects the degree of degradation and wear of the surface of the samples after wear tests. The general view of the observed changes in the coefficient of dry friction indicates the effect of structural changes on the change in the strength properties of alloys subjected to irradiation. It should also be noted that the presence of fluctuations in the values of the coefficient of dry friction in the range not exceeding 1–2% was associated with microstructural defects on the surface of the samples that can create obstacles during testing. As can be seen from the data presented, in the case of the initial sample of the alloy during the entire cycle of wear resistance tests, an increase in the friction coefficient was not observed, which indicates a high resistance of the alloy to wear resistance and external pressure during friction. In the case of irradiated samples, at low irradiation fluences of 10^{10} – 10^{11} ion/cm², there were practically no significant differences in the coefficient of dry friction, which also indicates a high resistance of the alloys to deformation fracture during testing. A slight increase in the coefficient of dry friction after 8000 test cycles for a sample irradiated with a fluence of 10^{11} ion/cm² indicates a slight decrease in the wear resistance of irradiated samples after long-term testing. Such an increase in the coefficient of dry friction was associated with the accumulation of deformation distortions in the structure of the damaged layer, which, under prolonged external action, can initiate partial embrittlement of the near-surface layer, thereby increasing friction and initiating surface wear, which is also clearly seen when evaluating the wear profile.

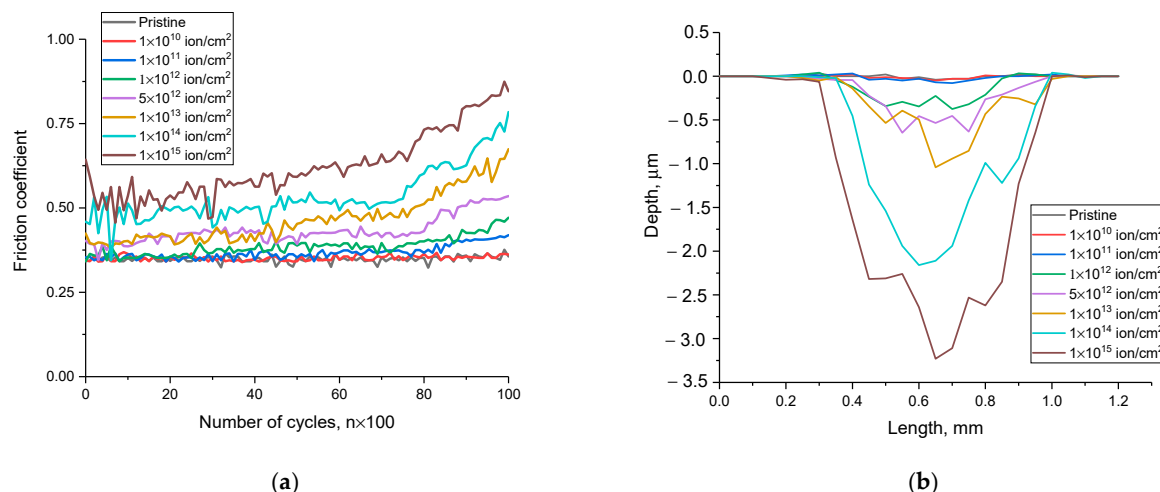


Figure 10. (a) Results of tribological tests to determine the coefficient of dry friction; (b) evaluation of the profile of the damaged layer after tests to determine the coefficient of dry friction.

An increase in the irradiation fluence above 10^{11} ions/cm² lead to an increase in the initial value of the dry friction coefficient, which was associated with the formation of deformation inclusions in the near-surface layer during the accumulation of radiation damage. At the same time, changes during long-term wear resistance tests indicate that deformation inclusions not only affected the increase in the friction coefficient after 7000–8000 cyclic tests, but also lead to an increase in the depth of the trace profile from the rubbing body, as well as its width. Such a change in the profile indicates destructive wear of the near-surface layer and its embrittlement, which lead to an increase in surface wear.

At irradiation fluences of 10^{14} – 10^{15} ion/cm², the initial value of the dry friction coefficient increased by 50–70% compared to the initial value, which indicates an increase in the concentration of deformation inclusions in the near-surface layer, which increase the friction resistance. It is also worth noting that surface degradation during long-term testing occurs much earlier for these irradiation fluences, which indicates the destructive nature of the accumulated damage in the near-surface layer, leading not only to bulk swelling, but also to rapid wear of the surface (see the data on changes in the depth profile in Figure 10b).

Figure 11 shows the results of changing the value of the coefficient of dry friction before and after testing, as well as the value of the wear rate of the damaged near-surface layer, depending on the amount of accumulated damage during irradiation with heavy ions. As can be seen from the data presented, the largest changes in the coefficient of dry friction, indicating the deterioration of the near-surface layer, both in the case of irradiated samples before and after cyclic tests, were observed with an increase in fluence above 5×10^{12} – 10^{13} ion/cm². Such a change in wear resistance at high irradiation fluences was due to the effects of accumulation of radiation damage and the formation of disordered regions in the damaged near-surface layer of alloys, which, according to X-ray diffraction data, lead to swelling and tensile deformation of the crystal lattice. The initialization of deformation distortions and their subsequent accumulation with an increase in the irradiation fluence lead to strength destabilization and partial softening of the damaged layer, which was more prone to destruction under prolonged external influences. At the same time, the presented dependence of the wear rate on the value of atomic displacements indicates that with the accumulation of deformation distortions, the wear rate somewhat decreases. This may be due to the fact that wear at high irradiation fluences began to occur with an increase in the damage volume, which was expressed both in an increase in the width of the damaged area and its depth.

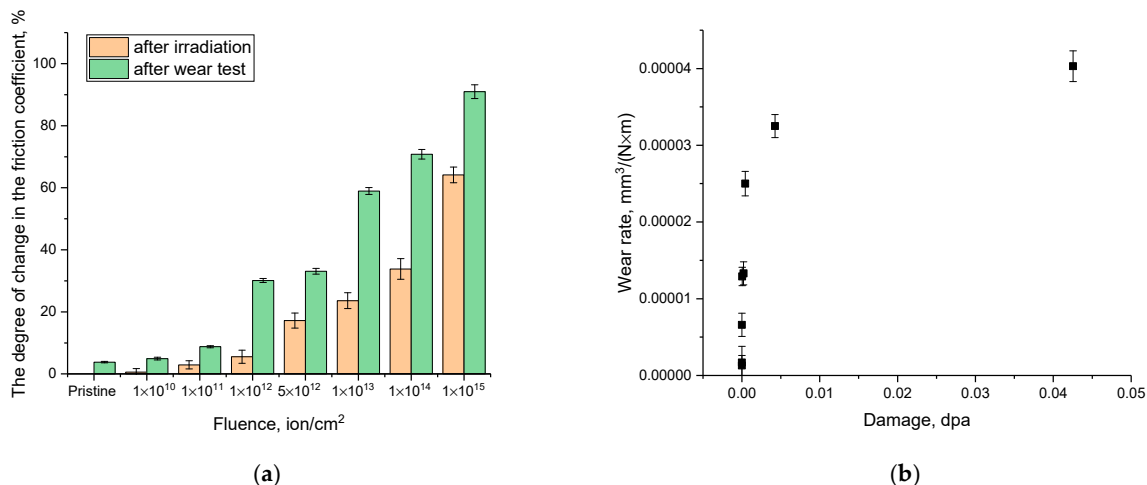


Figure 11. (a) Diagram of the change in the dry friction coefficient after irradiation in comparison with the initial value of the coefficient of friction for non-irradiated samples and after cyclic tests; (b) results of evaluation of changes in the wear rate with the accumulation of atomic displacements.

Thus, by analyzing the data on changes in the tribological and strength characteristics of the studied NbTiVZr alloys depending on the irradiation fluence and the amount of accumulated radiation damage, we can draw the following conclusion. Based on the fact that with the accumulation of radiation damage in the structure of the damaged layer, it swells, with a subsequent increase in volume, some of the formed defects are squeezed out to the surface, forming additional distortions in the form of swellings or microcracks [39]. At the same time, a change in the dislocation density due to size effects associated with a change in the orientation of the grains or their crushing, an increased content of dislocations is formed near the grain boundaries, which, under external influence (for example, friction), can lead to the emergence of metastable states capable of forming microcracks, the formation of which reduces crack resistance.

In this case, despite the increase in the wear rate during the accumulation of radiation damage in the near-surface layer, the wear rate remained comparable with similar wear rates for high-entropy alloys (TiZrNb)₁₄AlMo and CoCrFeNiMn, the test results of which are presented in review [40].

The obtained results of radiation damage in the course of the experiments carried out indicate that the greatest change was observed after reaching the radiation fluences

above 10^{13} ion/cm². These changes were expressed in the swelling of the crystal lattice due to the accumulation of radiation damage and atomic displacements, the accumulation of which occurred when the defect regions formed along the trajectory of charged ions overlap. At the same time, according to the fundamental work by Gary S. Was [38], the accumulation of radiation damage can be described using various models, as well as using molecular dynamics methods. The explanation of large structural changes, in particular, swelling and a decrease in strength properties, as well as resistance to degradation, can be explained by an increase in the magnitude of atomic displacements associated with the formation of cascade collisions of primary knocked-on atoms, which have high kinetic energy after collisions with incident particles. In this case, the overlap of defective regions with an increase in the irradiation fluence lead to the formation of strongly deformed regions in the structure of the damaged layer, with a high degree of anisotropy of the electron density distribution, the change in which can be explained by the redistribution of electrons along the ion trajectory in the material [38], since the dominant contribution to structural distortions was made by the interactions of incident particles with the electron subsystem for high-energy particles. An increase in the value of atomic displacements lead to deformation distortions of the structure, which, according to the presented data on changes in structural features, at high irradiation fluences, lead to partial amorphization of the damaged layer, which is associated with disordering of the structure at high values of atomic displacements and cascade collisions [31,38].

4. Conclusions

This article presented the results of an assessment of the structural and strength changes in NbTiVZr high-entropy alloy upon irradiation with heavy Kr¹⁵⁺ ions, comparable in energy to nuclear fuel fission fragments. Characterization of irradiation-induced changes in the near-surface layer of the alloys was carried out using the methods of X-ray diffraction analysis, indentation and determination of the dry friction coefficient. According to the estimated data of ionization losses, the main contribution to changes in the properties of the near-surface layer was made by the interactions of incident ions with the electron subsystem, which, in turn, lead to the appearance of nonequilibrium states with a changed electron density, leading to deformation distortions. An analysis of the structural changes caused by irradiation showed that the main contribution to the deterioration of the structural properties of the damaged layer was made by deformation tensile distortions, and at high irradiation fluences, amorphous inclusions appeared, which were formed during the accumulation of radiation damage. According to the presented data on the change in strength characteristics, a relationship between the accumulation of amorphous inclusions in the near-surface layer of alloys and softening was established. At the same time, the most pronounced changes in strength characteristics appeared at fluences above 10^{13} ion/cm².

Author Contributions: Conceptualization, V.V.U., D.I.S., D.B.B., K.K.K. and A.L.K.; methodology, S.G.G., V.V.U., M.V.Z. and A.L.K.; formal analysis, M.V.Z., D.I.S. and A.L.K.; investigation, V.V.U., S.G.G., M.V.Z., K.K.K., D.I.S. and A.L.K.; resources, A.L.K.; writing—original draft preparation, review, and editing, D.I.S. and A.L.K.; visualization, A.L.K.; supervision, A.L.K. All authors have read and agreed to the published version of the manuscript.

Funding: This research was funded by the Science Committee of the Ministry of Education and Science of the Republic of Kazakhstan (No. BR18574135).

Institutional Review Board Statement: Not applicable.

Informed Consent Statement: Not applicable.

Data Availability Statement: Not applicable.

Conflicts of Interest: The authors declare no conflict of interest.

References

1. Féron, D. Overview of nuclear materials and nuclear corrosion science and engineering. In *Nuclear Corrosion Science and Engineering*; Woodhead Publishing: Sawston, UK, 2012; pp. 31–56.
2. Zinkle, S.; Terrani, K.; Snead, L. Motivation for utilizing new high-performance advanced materials in nuclear energy systems. *Curr. Opin. Solid State Mater. Sci.* **2016**, *20*, 401–410. [[CrossRef](#)]
3. Konings, R.; Stoller, R. *Comprehensive Nuclear Materials*; Elsevier: Amsterdam, The Netherlands, 2020.
4. Buckthorpe, D. Introduction to Generation IV nuclear reactors. In *Structural Materials for Generation IV Nuclear Reactors*; Woodhead Publishing: Sawston, UK, 2017; pp. 1–22.
5. Zohuri, B. Generation IV nuclear reactors. In *Nuclear Reactor Technology Development and Utilization*; Woodhead Publishing: Sawston, UK, 2020; pp. 213–246.
6. Şahin, S.; Şahin, H.M. Generation-IV reactors and nuclear hydrogen production. *Int. J. Hydrog. Energy* **2021**, *46*, 28936–28948. [[CrossRef](#)]
7. Henry, J.; Maloy, S. Irradiation-resistant ferritic and martensitic steels as core materials for Generation IV nuclear reactors. In *Structural Materials for Generation IV Nuclear Reactors*; Woodhead Publishing: Sawston, UK, 2017; pp. 329–355.
8. Marsden, B.; Jones, A.; Hall, G.; Treifi, M.; Mummary, P. Graphite as a core material for Generation IV nuclear reactors. In *Structural Materials for Generation IV Nuclear Reactors*; Woodhead Publishing: Sawston, UK, 2017; pp. 495–532.
9. Mansur, L.K.; Rowcliffe, A.F.; Nanstad, R.K.; Zinkle, S.J.; Corwin, W.R.; Stoller, R.E. Materials needs for fusion, Generation IV fission reactors and spallation neutron sources—similarities and differences. *J. Nucl. Mater.* **2004**, *329*, 166–172. [[CrossRef](#)]
10. Pioro, I. (Ed.) *Handbook of Generation IV Nuclear Reactors: A Guidebook*; Woodhead Publishing: Sawston, UK, 2022.
11. Gong, X.; Short, M.P.; Auger, T.; Charalampopoulou, E.; Lambrinou, K. Environmental degradation of structural materials in liquid lead-and lead-bismuth eutectic-cooled reactors. *Prog. Mater. Sci.* **2022**, *1*, 100920. [[CrossRef](#)]
12. Eswarappa Prameela, S.; Pollock, T.M.; Raabe, D.; Meyers, M.A.; Aitkaliyeva, A.; Chintersingh, K.L.; Cordero, Z.C.; Graham-Brady, L. Materials for extreme environments. *Nat. Rev. Mater.* **2023**, *8*, 81–88. [[CrossRef](#)]
13. Marques, J. Evolution of nuclear fission reactors: Third generation and beyond. *Energy Convers. Manag.* **2010**, *51*, 1774–1780. [[CrossRef](#)]
14. Locatelli, G.; Mancini, M.; Todeschini, N. Generation IV nuclear reactors: Current status and future prospects. *Energy Policy* **2013**, *61*, 1503–1520. [[CrossRef](#)]
15. Gul, A.O.; Kavaz, E.; Basgoz, O.; Guler, O.; ALMisned, G.; Bahceci, E.; Albayrak, M.G.; Tekin, H.O. Newly synthesized NiCoFeCrW High-Entropy Alloys (HEAs): Multiple impacts of B4C additive on structural, mechanical, and nuclear shielding properties. *Intermetallics* **2022**, *146*, 107593. [[CrossRef](#)]
16. Pickering, E.J.; Carruthers, A.W.; Barron, P.J.; Middleburgh, S.C.; Armstrong, D.E.; Gandy, A.S. High-Entropy Alloys for Advanced Nuclear Applications. *Entropy* **2021**, *23*, 98. [[CrossRef](#)]
17. Moschetti, M.; Burr, P.A.; Obbard, E.; Krizic, J.J.; Hosemann, P.; Gludovatz, B. Design considerations for high entropy alloys in advanced nuclear applications. *J. Nucl. Mater.* **2022**, *567*, 153814. [[CrossRef](#)]
18. Kareer, A.; Waite, J.C.; Li, B.; Couet, A.; Armstrong, D.E.J.; Wilkinson, A.J. Low activation, refractory, high entropy alloys for nuclear applications. *J. Nucl. Mater.* **2019**, *526*, 151744. [[CrossRef](#)]
19. Xia, S.-Q.; Wang, Z.; Yang, T.-F.; Zhang, Y. Irradiation Behavior in High Entropy Alloys. *J. Iron Steel Res. Int.* **2015**, *22*, 879–884. [[CrossRef](#)]
20. Xiang, C.; Han, E.-H.; Zhang, Z.; Fu, H.; Wang, J.; Zhang, H.; Hu, G. Design of single-phase high-entropy alloys composed of low thermal neutron absorption cross-section elements for nuclear power plant application. *Intermetallics* **2019**, *104*, 143–153. [[CrossRef](#)]
21. Voyevodin, V.; Tolstolutskaya, G.; Tikhonovsky, M.; Kuprin, A.; Kalchenko, A. Mechanisms of radiation damage and development of structural materials for operating and advanced nuclear reactors. *Probl. At. Sci. Technol.* **2021**, *135*, 3–20. [[CrossRef](#)]
22. Daghbouj, N.; Li, B.; Callisti, M.; Sen, H.S.; Karlik, M.; Polcar, T. Microstructural evolution of helium-irradiated 6H-SiC subjected to different irradiation conditions and annealing temperatures: A multiple characterization study. *Acta Mater.* **2019**, *181*, 160–172. [[CrossRef](#)]
23. Aizenshtein, M.; Ungarish, Z.; Woller, K.; Hayun, S.; Short, M. Mechanical and microstructural response of the Al0.5CoCrFeNi high entropy alloy to Si and Ni ion irradiation. *Nucl. Mater. Energy* **2020**, *25*, 100813. [[CrossRef](#)]
24. Yao, H.W.; Qiao, J.W.; Gao, M.C.; Hawk, J.A.; Ma, S.G.; Zhou, H.F.; Zhang, Y. NbTaV-(Ti,W) refractory high-entropy alloys: Experiments and modeling. *Mater. Sci. Eng. A* **2016**, *674*, 203–211. [[CrossRef](#)]
25. Chen, S.; Tong, Y.; Tseng, K.-K.; Yeh, J.-W.; Poplawsky, J.; Wen, J.; Gao, M.; Kim, G.; Chen, W.; Ren, Y.; et al. Phase transformations of HfNbTaTiZr high-entropy alloy at intermediate temperatures. *Scr. Mater.* **2019**, *158*, 50–56. [[CrossRef](#)]
26. Whitfield, T.E.; Pickering, E.J.; Christofidou, K.A.; Jones, C.N.; Stone, H.J.; Jones, N.G. Elucidating the microstructural development of refractory metal high entropy superalloys via the Ti-Ta-Zr constituent system. *J. Alloy. Compd.* **2020**, *818*, 152935. [[CrossRef](#)]
27. King, D.; Cheung, S.; Humphry-Baker, S.A.; Parkin, C.; Couet, A.; Cortie, M.B.; Lumpkin, G.R.; Middleburgh, S.C.; Knowles, A.J. High temperature, low neutron cross-section high-entropy alloys in the Nb-Ti-V-Zr system. *Acta Mater.* **2019**, *166*, 435–446. [[CrossRef](#)]
28. Cheng, Z.; Sun, J.; Gao, X.; Wang, Y.; Cui, J.; Wang, T.; Chang, H. Irradiation effects in high-entropy alloys and their applications. *J. Alloys Compd.* **2022**, *930*, 166768. [[CrossRef](#)]

29. Xia, S.; Gao, M.C.; Yang, T.; Liaw, P.K.; Zhang, Y. Phase stability and microstructures of high entropy alloys ion irradiated to high doses. *J. Nucl. Mater.* **2016**, *480*, 100–108. [[CrossRef](#)]
30. Wang, X.; Zhang, H.; Baba, T.; Jiang, H.; Liu, C.; Guan, Y.; Elleuch, O.; Kuech, T.; Morgan, D.; Idrobo, J.-C.; et al. Radiation-induced segregation in a ceramic. *Nat. Mater.* **2020**, *19*, 992–998. [[CrossRef](#)] [[PubMed](#)]
31. Williford, R.E.; Devanathan, R.; Weber, W.J. Computer simulation of displacement energies for several ceramic materials. *Nucl. Instrum. Methods Phys. Res. Sect. B Beam Interact. Mater. At.* **1998**, *141*, 94–98. [[CrossRef](#)]
32. Fellman, A.; Sand, A. Recoil energy dependence of primary radiation damage in tungsten from cascade overlap with voids. *J. Nucl. Mater.* **2022**, *572*, 154020. [[CrossRef](#)]
33. Huang, X.; Yi, J.; Ding, J.; Song, K.; Lu, S.; Liu, H.; Wang, L. Radiation damage behavior and mechanism in RAFM steel: Orientation effect. *Vacuum* **2022**, *205*, 111445. [[CrossRef](#)]
34. Andreoli, A.F.; Mendes, R.G.; Witusiewicz, V.T.; Shuleshova, O.; van Huis, M.A.; Nielsch, K.; Kaban, I. Phase constitution and microstructure of the NbTiVZr refractory high-entropy alloy solidified upon different processing. *Acta Mater.* **2021**, *221*, 117416. [[CrossRef](#)]
35. Daghbouj, N.; Sen, H.; Callisti, M.; Vronka, M.; Karlik, M.; Duchoň, J.; Čech, J.; Havránek, V.; Polcar, T. Revealing nanoscale strain mechanisms in ion-irradiated multilayers. *Acta Mater.* **2022**, *229*, 117807. [[CrossRef](#)]
36. Liu, K.; Zhang, K.; Deng, T.; Li, W.; Zhang, H. Comparative study of irradiation effects on nanosized and microsized $\text{Gd}_2\text{Zr}_2\text{O}_7$ ceramics. *Ceram. Int.* **2020**, *46*, 16987–16992. [[CrossRef](#)]
37. Daghbouj, N.; Sen, H.S.; Čížek, J.; Lorinčík, J.; Karlik, M.; Callisti, M.; Polcar, T. Characterizing heavy ions-irradiated Zr/Nb: Structure and mechanical properties. *Mater. Des.* **2022**, *219*, 110732. [[CrossRef](#)]
38. Was, G.S. *Fundamentals of Radiation Materials Science: Metals and Alloys*; Springer: Berlin/Heidelberg, Germany, 2016.
39. AlMotasem, A.; Daghbouj, N.; Sen, H.; Mirzaei, S.; Callisti, M.; Polcar, T. Influence of HCP/BCC interface orientation on the tribological behavior of Zr/Nb multilayer during nanoscratch: A combined experimental and atomistic study. *Acta Mater.* **2023**, *249*, 118832. [[CrossRef](#)]
40. Zhou, J.-L.; Yang, J.-Y.; Zhang, X.-F.; Ma, F.-W.; Ma, K.; Cheng, Y.-H. Research status of tribological properties optimization of high-entropy alloys: A review. *J. Mater. Sci.* **2023**, *58*, 4257–4291. [[CrossRef](#)]

Disclaimer/Publisher’s Note: The statements, opinions and data contained in all publications are solely those of the individual author(s) and contributor(s) and not of MDPI and/or the editor(s). MDPI and/or the editor(s) disclaim responsibility for any injury to people or property resulting from any ideas, methods, instructions or products referred to in the content.